Journal of Zhejiang University-SCIENCE A (Applied Physics & Engineering) 2024 25(11):922-937
www.jzus.zju.edu.cn; www.springer.com/journal/11582
E-mail: jzus_a@zju.edu.cn

Research Article

https://doi.org/10.1631/jzus.A2300340

Efficient reliability analysis via a nonlinear autoregressive multi-fidelity surrogate model and active learning

Yifan LI, Yongyong XIANG, Luojie SHI, Baisong PAN✉

College of Mechanical Engineering, Zhejiang University of Technology, Hangzhou 310023, China

Abstract: For complex engineering problems, multi-fidelity modeling has been used to achieve efficient reliability analysis by leveraging multiple information sources. However, most methods require nested training samples to capture the correlation between different fidelity data, which may lead to a significant increase in low-fidelity samples. In addition, it is difficult to build accurate surrogate models because current methods do not fully consider the nonlinearity between different fidelity samples. To address these problems, a novel multi-fidelity modeling method with active learning is proposed in this paper. Firstly, a nonlinear autoregressive multi-fidelity Kriging (NAMK) model is used to build a surrogate model. To avoid introducing redundant samples in the process of NAMK model updating, a collective learning function is then developed by a combination of a U-learning function, the correlation between different fidelity samples, and the sampling cost. Furthermore, a residual model is constructed to automatically generate low-fidelity samples when high-fidelity samples are selected. The efficiency and accuracy of the proposed method are demonstrated using three numerical examples and an engineering case.

Key words: Reliability analysis; Multi-fidelity surrogate model; Active learning; Nonlinearity; Residual model

1 Introduction

Reliability analysis plays a critical role in engineering design, as it aims to assess the probability of system failure with respect to specific performance criteria, considering the presence of various uncertainties (Echard et al., 2013). Generally, the failure probability can be calculated by a multi-dimensional integral:

$$p_f = \int_{G(\boldsymbol{x})<0} f_x(\boldsymbol{x})\,\mathrm{d}\boldsymbol{x}, \tag{1}$$

where $\boldsymbol{x}=[x_1, x_2, \ldots, x_n]^{\mathrm{T}}$ denotes all random input variables, $f_x(\boldsymbol{x})$ is the joint probability density function of $\boldsymbol{x}$, and $G(\boldsymbol{x})$ represents the limit state function.

In practical engineering scenarios, the analytical solution of the above integral may not be obtained because limit state functions are usually implicit (Schuëller and Pradlwarter, 2007). The Monte Carlo simulation (MCS) method is a robust tool to deal with this problem. Nonetheless, a key limitation of MCS is the need for extensive limit state function evaluations to precisely estimate failure probabilities. Especially for complex problems which need finite element analysis, the total computational budget is unaffordable (Lelièvre et al., 2018). Some novel sampling methods, for example, importance sampling (IS) (Melchers, 1990; Papaioannou et al., 2016) and subset simulation (SS) (Song et al., 2009; Li and Cao, 2016), have been developed to enhance the efficiency of MCS, but they still require a substantial number of calls to the limit state function to obtain the failure probability with a satisfactory level of accuracy. Most probable point (MPP)-based methods, such as the first-order reliability method (FORM) (Hohenbichler and Rackwitz, 1982) and second-order reliability method (SORM) (Kiureghian and Stefano, 1991), are frequently used to perform effective reliability analysis. However, these methods may have large errors when dealing with scenarios involving multiple MPPs or highly nonlinear limit state functions (Gavin and Yau, 2008). Moment-based methods (Hong, 1996; Zhang and Pandey, 2013), which reconstruct the actual limit state probability

✉ Baisong PAN, panbsz@zjut.edu.cn
Baisong PAN, https://orcid.org/0000-0002-5688-9086

Received July 2, 2023; Revision accepted Jan. 23, 2024
Crosschecked Sept. 11, 2024; Online first Nov. 21, 2024

density function from statistical moments derived from sampling, depend heavily on the choice of a suitable statistical model for their accuracy.

Recently, surrogate models have gained widespread popularity in reliability analysis, primarily due to their capability to handle problems characterized by complex implicit limit state functions. These models enable numerous simulation runs at a limited computational cost, facilitating failure probability evaluations (Aldosary et al., 2018; Wang et al., 2021). Representative surrogate models include response surface methodology (RSM) (Rajashekhar and Ellingwood, 1993; Goswami et al., 2016), polynomial chaos expansion (PCE) (Hu and Youn, 2011; He et al., 2020), support vector regression (SVR) (Feng et al., 2019; Roy et al., 2019), radial basis function (RBF) (Li et al., 2018), Kriging (also called Gaussian process) (Kaymaz, 2005; Su et al., 2017; Zhou and Peng, 2020b), and artificial neural network (ANN) (Cheng and Li, 2008; Ren et al., 2022). Accurate failure probability estimation by these models necessitates precise classification of samples as failing or non-failing, particularly near the limit state boundary. Therefore, various active learning strategies have been proposed to select samples adaptively and update the surrogate model efficiently. Efficient global reliability analysis (EGRA) (Bichon et al., 2008), active Kriging Monte Carlo simulation (AK-MCS) (Echard et al., 2011), and importance sampling and Kriging reliability method (AK-IS) (Echard et al., 2013) are the most popular active learning methods. Based on these methods, numerous enhanced methodologies, such as reliability analysis through error rate-based adaptive Kriging (REAK) (Wang and Shafieezadeh, 2019b), adaptive Kriging-oriented importance sampling (AKOIS) (Zhang et al., 2020), and the surrogate model-based active learning method (SM-ALM) (Hong et al., 2022), have been developed to achieve notable efficiency and accuracy for scenarios with multiple failure areas and low failure probabilities. However, for certain complex engineering challenges, such as aerodynamic simulations (Zhao et al., 2019) and vehicle collision analyses (Wu et al., 2019), their computational intensity poses a significant challenge in acquiring sufficient high-fidelity samples for constructing accurate surrogate models, especially under limited simulation resources.

Multi-fidelity surrogate-based methods provide a feasible way to reduce the computational cost of these reliability analysis problems. Although some low-fidelity models may have significant errors (e.g., simplified physical and coarse mesh models), low-fidelity samples can still provide some useful information, such as the changing trend of the response (Forrester et al., 2007; Guo et al., 2022). Consequently, it is crucial for multi-fidelity modeling to effectively capture the relationship between high-fidelity and low-fidelity responses. In recent years, a variety of multi-fidelity modeling approaches, including the co-Kriging (Forrester et al., 2007), the nonlinear autoregressive scheme (Perdikaris et al., 2017), and the multi-fidelity deep Gaussian process (MF-DGP) scheme (Cutajar et al., 2019), have been developed. However, compared to active learning-based modeling methods, building a multi-fidelity model using a one-shot sampling strategy may significantly increase the computational cost due to the incomplete use of information. Thus, researchers are increasingly incorporating active learning into multi-fidelity scenarios, leveraging the benefits of multi-fidelity modeling while adaptively selecting new samples near failure domains for continuous model enhancement. For instance, Chaudhuri et al. (2021) proposed a multi-fidelity efficient global reliability analysis (mfEGRA) approach that combines the EGRA method with the multi-information source optimization method. To enhance the applicability of co-Kriging modeling in predicting the limit state function for reliability analysis, Liu et al. (2022) developed an extended expected improvement (EEI) infill criterion. Yi et al. (2021) proposed a learning function called the augmented expected feasibility (AEF) function for multi-fidelity modeling to reduce the computational burden of reliability analysis. To effectively capture the correlations between data with different fidelities, nested samples are commonly used to build surrogate models (Meng and Karniadakis, 2020; Chen et al., 2022). This leads to a huge number of low-fidelity samples. Besides, existing multi-fidelity surrogate-based modeling methods often use a scaling factor and an error term to represent the relationship between different fidelity samples. However, the scaling factor and error term cannot completely consider possible nonlinear relationships, which may lead to an incorrect trend and unreliable predictions.

In this paper, we present a multi-fidelity surrogate modeling scheme combined with active learning to attain efficient reliability analysis with high accuracy.

The primary research developments concern the following three aspects: (1) To improve the model's ability to represent the relationship between information with different fidelities, we introduce the nonlinear autoregressive scheme (Perdikaris et al., 2017) and construct a multi-fidelity surrogate named the nonlinear autoregressive multi-fidelity Kriging (NAMK) model. (2) In the process of model refinement, the traditional learning function is replaced by a collective multi-fidelity learning function, which selects new sampling points from the multi-fidelity sample space by comprehensively considering the sampling cost and the correlation between multi-fidelity samples. (3) To further reduce the number of samples, instead of directly sampling, nested low-fidelity samples are generated using a constructed residual model when selecting high-fidelity samples.

The remainder of the paper is organized as follows. A brief review of the basic theory of the proposed approach is given in Section 2. Section 3 introduces the proposed method in detail. Three numerical examples and an engineering case are provided in Section 4 to show the applicability of the proposed method. Conclusions are summarized in Section 5.

2 Foundational concepts

2.1 Kriging model

A Kriging model leverages the information from multiple samples to fit the original model, thereby enabling the estimation of responses and quantification of uncertainties for any given sampling point (Krige, 1951). A Kriging model can be formulated by

$$\hat{g}(\boldsymbol{x})=\boldsymbol{h}(\boldsymbol{x})^{\mathrm{T}}\boldsymbol{\beta}+Z(\boldsymbol{x}), \tag{2}$$

where $\boldsymbol{h}(\boldsymbol{x})=[h_1(\boldsymbol{x}), h_2(\boldsymbol{x}), \ldots, h_k(\boldsymbol{x})]$ is the basis function, $\boldsymbol{\beta}=[\beta_1, \beta_2, \ldots, \beta_k]$ is the vector of regression coefficients, and $Z(\boldsymbol{x})$ is a Gaussian process characterized by a zero mean and a covariance:

$$\mathrm{Cov}[Z(\boldsymbol{a}), Z(\boldsymbol{b})]=\sigma_Z^2\boldsymbol{K}(\boldsymbol{a}, \boldsymbol{b}), \tag{3}$$

where σ_Z^2 denotes the variance of $Z(\boldsymbol{x})$; $\boldsymbol{a}$ and $\boldsymbol{b}$ are two points of the Gaussian process; $\boldsymbol{K}(\boldsymbol{a}, \boldsymbol{b})$ represents the covariance matrix and can be commonly defined as multiple forms. The Gaussian correlation function was used in this study because of its robustness and suitability (Jones et al., 1998). For an unknown point $\boldsymbol{x}^*$, its predicted value $\hat{G}(\boldsymbol{x}^*)$ and variance $\hat{\sigma}_{\hat{G}}^2(\boldsymbol{x}^*)$ are expressed as

$$\hat{G}(\boldsymbol{x}^*)=\hat{\beta}+\boldsymbol{r}^{\mathrm{T}}(\boldsymbol{x}^*)\boldsymbol{K}^{-1}\left(Y-\hat{\beta}\boldsymbol{1}\right), \tag{4}$$

$$\hat{\sigma}_{\hat{G}}^2(\boldsymbol{x}^*)=\sigma_Z^2\left(1+\boldsymbol{u}^{\mathrm{T}}(\boldsymbol{1}^{\mathrm{T}}\boldsymbol{K}^{-1}\boldsymbol{1})^{-1}\boldsymbol{u}-\boldsymbol{r}^{\mathrm{T}}(\boldsymbol{x}^*)\boldsymbol{K}^{-1}\boldsymbol{r}(\boldsymbol{x}^*)\right), \tag{5}$$

where $\hat{\beta}$ is an estimate of the mean; Y is the observed value for known points; $\boldsymbol{K}^{-1}$ is the inverse matrix of the covariance matrix $\boldsymbol{K}$ of known points; $\boldsymbol{r}^{\mathrm{T}}(\boldsymbol{x}^*)=\left[\boldsymbol{K}(\boldsymbol{x}^*, \boldsymbol{x}^{(1)}), \boldsymbol{K}(\boldsymbol{x}^*, \boldsymbol{x}^{(2)}), \ldots, \boldsymbol{K}(\boldsymbol{x}^*, \boldsymbol{x}^{(p)})\right]^{\mathrm{T}}$, and $\boldsymbol{u}=\boldsymbol{1}^{\mathrm{T}}\boldsymbol{K}^{-1}\boldsymbol{r}^{\mathrm{T}}(\boldsymbol{x}^*)-1$.

2.2 Multi-fidelity modeling method

The objective of the multi-fidelity modeling method is to establish a mapping relationship between low-fidelity and high-fidelity responses by creating a joint model that integrates multi-source information (Kennedy and O'Hagan, 2000; Le Gratiet and Garnier, 2014). In our research, we used a nonlinear autoregressive scheme (Perdikaris et al., 2017) to capture the relationship between multi-fidelity data because of its excellent nonlinear characterization performance. The nonlinear autoregressive scheme constructs a nested input structure by incorporating the response of low-fidelity samples into the input of the high-fidelity model. Compared with the MF-DGP scheme (Cutajar et al., 2019), the nonlinear autoregressive scheme trains each fidelity-level model independently, resulting in low computational complexity and flexible modeling.

Suppose there are sample sets $D_m=[\boldsymbol{X}_m, Y_m]$ with increasing fidelity m (m=1, 2, ⋯, H, where H is the highest fidelity level). The nonlinear autoregressive multi-fidelity model is given by

$$g_m(\boldsymbol{x})=Q_m([\boldsymbol{x}, g_{m-1}(\boldsymbol{x})]), \tag{6}$$

where $g_m(\boldsymbol{x})$ is the surrogate model constructed by the samples with fidelity level m, and $Q_m\sim \mathrm{GP}\left(g_m|\boldsymbol{0}, \boldsymbol{r}_m\left((\boldsymbol{x}, g_{m-1}(\boldsymbol{x})), (\boldsymbol{x}^{\mathrm{T}}, g_{m-1}(\boldsymbol{x}^{\mathrm{T}}))\right); \boldsymbol{\theta}_m\right)$. $Q_m(\cdot)$ can more fully represent the relationship between

samples with different fidelities, and its covariance kernel is given by

$$\boldsymbol{K}_{m_g}=\boldsymbol{K}_{m_\rho}\left(\boldsymbol{x},\,\boldsymbol{x}^{\mathrm{T}};\,\boldsymbol{\theta}_{m_\rho}\right)\times\boldsymbol{K}_{m_t}(g_{m-1}(\boldsymbol{x}),\,g_{m-1}(\boldsymbol{x}^{\mathrm{T}});\,\boldsymbol{\theta}_{m_t})+\boldsymbol{K}_{m_\delta}(\boldsymbol{x},\,\boldsymbol{x}^{\mathrm{T}};\,\boldsymbol{\theta}_{m_\delta}),\tag{7}$$

where $\boldsymbol{K}_{m_\rho}$, $\boldsymbol{K}_{m_t}$, and $\boldsymbol{K}_{m_\delta}$ are covariance functions and $\boldsymbol{\theta}_m=\left[\boldsymbol{\theta}_{m_\rho},\,\boldsymbol{\theta}_{m_t},\,\boldsymbol{\theta}_{m_\delta}\right]$ expresses their hyperparameters.

3 Proposed method

In this section, the surrogate-based reliability framework using an NAMK model and active learning is presented. The core strategy involves establishing an NAMK model using the nonlinear autoregressive scheme, followed by iterative refinement based on adaptively selected new samples. Firstly, initial multi-fidelity samples are selected in the specified parameter range and an initial surrogate model is constructed using NAMK. In the process of model updating, the position and fidelity of new samples are determined by a collective learning function. Once a high-fidelity sample is determined, a corresponding nested low-fidelity sample can be automatically generated according to a residual model. Finally, a stopping criterion using relative error estimation terminates the active learning process. Fig. 1 shows a flowchart of the approach.

3.1 Initial sample selection

The distribution of initial samples largely determines the performance of the surrogate model and the efficiency of the active learning process. When the initial samples are evenly filled in the design space, a comprehensive evaluation of the limit state function can be obtained. A Latin hypercube sampling method based on evolutionary operation (EVOP-LHS) (Forrester et al., 2008) is used to obtain initial low-fidelity samples $\{\boldsymbol{X}_m\}_{m=1}$ that are evenly distributed in the sample space. Then, an exchange algorithm (Reisenthel

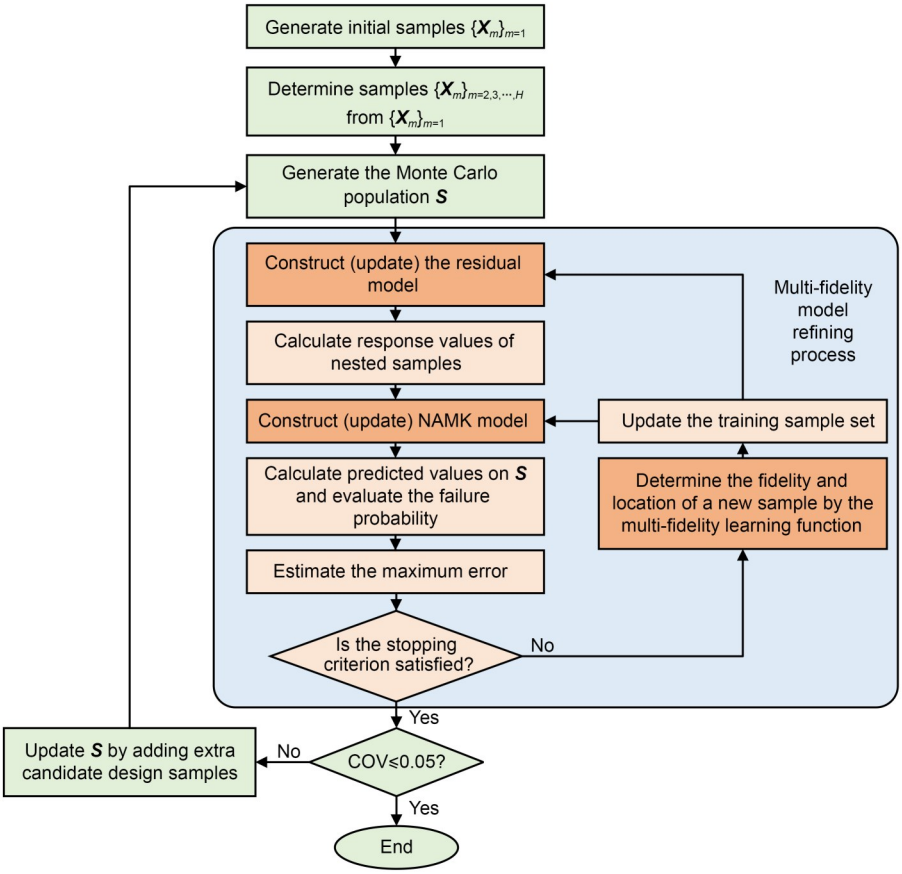

Fig. 1 Flowchart of the proposed approach. COV is the coefficient of variation

and Allen, 2014) is adopted to obtain the higher-fidelity samples $\{\boldsymbol{X}_m\}_{m=2,3,\cdots,H}$ to ensure the nesting property and distribution uniformity among samples with different fidelities.

3.2 Construction of the residual model and generation of the nested low-fidelity sample

In the case of a multi-fidelity surrogate model, when a nested relationship exists between training samples of different fidelity levels, the model can provide a more precise description of the relationship between the samples (Perdikaris et al., 2017; Liu et al., 2022). This nested relationship allows the model to capture the intricate connections and dependencies among the samples with greater accuracy. The nested relationship between training samples when $\boldsymbol{x}$ is one dimensional is presented in Fig. 2a. However, extra calculations are needed to obtain nested low-fidelity samples in the process of model updating (Fig. 2b).

In this study, a residual modeling method was used to generate nested low-fidelity samples. The core idea of residual modeling is to capture the discrepancy between the high-fidelity sample response values Y_m and the low-fidelity sample response values Y_{m-1} by constructing a residual model $F_{\mathrm{Re}}(\cdot)$. This model is then used to calculate the responses of the nested low-fidelity samples. The detailed construction process of the residual model can be found in Section S1 of the electronic supplementary materials (ESM).

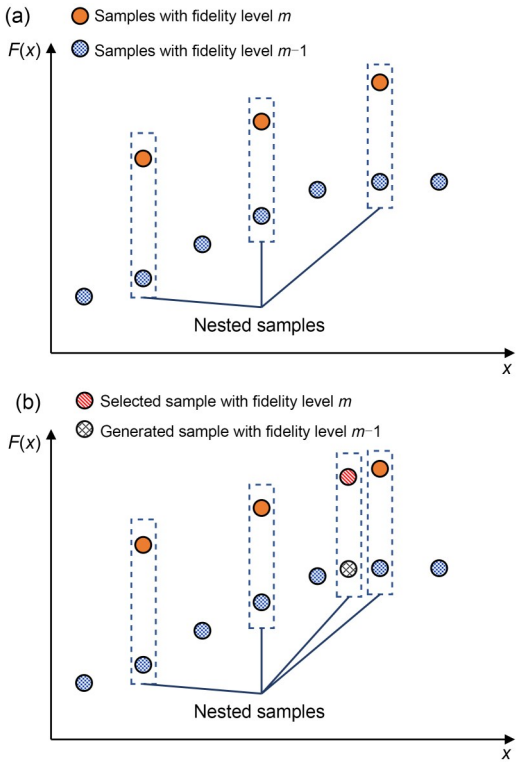

Fig. 2 Relationships between multi-fidelity samples: (a) nested multi-fidelity samples; (b) selected sample with fidelity level *m* and the generated sample with fidelity level *m*−1

3.3 Construction of the NAMK model and calculation of the predicted response value

The main goal of the multi-fidelity modeling strategy is to use nested multi-fidelity training samples $[\boldsymbol{X}_m,\ Y_m]_{m=1,2,\cdots,H}$ to capture the relationship $q_m(\cdot)$ between $g_m(\boldsymbol{x})$ and $g_{m-1}(\boldsymbol{x})$. In this study, the nonlinear autoregressive scheme (Perdikaris et al., 2017) was used to establish a multi-fidelity surrogate model in combination with a Kriging model since it can effectively capture the nonlinear relationship between different fidelity information by incorporating an additional input into the high-fidelity model.

An initial Kriging model $Z_{m=1}(\cdot)$ was constructed using the lowest-fidelity sample set $[\boldsymbol{X}_m,\ Y_m]_{m=1}$. After the sample set $[\boldsymbol{X}_m,\ Y_m]_{m=2}$ of the higher-fidelity level and predicted response values $\hat{G}_{m=1}(\boldsymbol{X}_{m=1})$ are obtained, $Z_{m=2}(\cdot)$ is built by

$$Y_{m=2}=Z_{m=2}\left(\boldsymbol{X}_{m=2},\ \hat{G}_{m=1}(\boldsymbol{X}_{m=1})\right). \tag{8}$$

From Eq. (8), it is known that $Z_{m=2}(\cdot)$ can not only accurately predict the response values $\boldsymbol{X}_{m=1}$, but also characterize the relationship between samples with fidelity m=1 and m=2.

Once $Z_{m=H}(\cdot)$ is determined using the highest-fidelity sample set $[\boldsymbol{X}_m,\ Y_m]_{m=H}$ and $\hat{G}(\boldsymbol{X}_{m=H-1})$, the NAMK model $V_{m=H}(\cdot)$ is formulated by an autoregressive form:

$$V_{m=H}(\boldsymbol{x})=\begin{cases}Z_{m=1}(\boldsymbol{x}),\\ Z_{m=2}\left(\boldsymbol{x},\ \hat{G}_{m=1}(\boldsymbol{x})\right),\\ \cdots\\ Z_{m=H}\left(\boldsymbol{x},\ \hat{G}_{m=H-1}(\boldsymbol{x})\right).\end{cases} \tag{9}$$

Predictive response values $\hat{G}_m(\boldsymbol{x}_i)$ of candidate samples can be calculated according to $V_{m=H}(\cdot)$, namely

$$\hat{G}_m(\boldsymbol{x}_i)=Z_m\left(\boldsymbol{x}_i,\ \hat{G}_{m-1}(\boldsymbol{x}_i)\right),\quad m=2,\ 3,\ \cdots,\ H,\quad (10)$$

where $\boldsymbol{x}_i\ (i=1,\ 2,\ \cdots,\ N_{\mathrm{MCS}})$ indicates candidate samples from Monte Carlo population $\boldsymbol{S}$, and N_{MCS} is the total number of samples in the Monte Carlo population.

3.4 Active learning strategy

3.4.1 Determination of new samples

A traditional learning function usually selects useful samples according to the posterior mean and standard deviation of candidate training samples, and is applicable only for active learning problems with a single information source scenario. For multi-source information, the site and fidelity of samples should be determined in the active learning process. In addition, models with different fidelities have different calculation costs, so the sampling cost also needs to be considered in the process of selecting new samples. Therefore, a new collective multi-fidelity learning function consisting of three parts is proposed to select suitable samples. The formulation of this learning function is

$$F_{\mathrm{MF}}(\boldsymbol{x},\ m)=U_{\mathrm{MF}}(\boldsymbol{x})\times C_{\mathrm{R}}(\boldsymbol{x},\ m)\times\frac{1}{c(m)},\quad m=1,\ 2,\ \cdots,\ H,\quad (11)$$

where $c(m)$ is the function of sampling cost, which is used to assess the relative computational cost associated with samples of different fidelities, and is usually expressed as

$$c(m)=\frac{T_{\mathrm{c}}(m)}{T_{\mathrm{c}}(H)},\quad m=1,\ 2,\ \cdots,\ H,\quad (12)$$

where $T_{\mathrm{c}}(\cdot)$ represents the calculation time required to obtain the sample response. $U_{\mathrm{MF}}(\boldsymbol{x})$ represents the expected feasibility of candidate points under different fidelities. Its function can be obtained by extending the U-learning function (Echard et al., 2011), i.e.,

$$U_{\mathrm{MF}}(\boldsymbol{x})=\frac{\sigma_{\hat{G}_m}(\boldsymbol{x})}{\left|\hat{G}_H(\boldsymbol{x})\right|},\quad m=1,\ 2,\ \cdots,\ H,\quad (13)$$

where $\sigma_{\hat{G}_m}(\boldsymbol{x})$ represents the posterior standard deviation of samples with fidelity level m, and $\hat{G}_H(\boldsymbol{x})$ is the response of the highest-fidelity model corresponding to the current sample. Using $U_{\mathrm{MF}}(\boldsymbol{x})$, these candidates, which are characterized by their proximity to the high-fidelity limit state function and high uncertainty, can be effectively identified and selected. $C_{\mathrm{R}}(\boldsymbol{x},\ m)$ represents the relative correlation of multi-fidelity samples, which depends mainly on the predicted response and posterior variance (Reisenthel and Allen, 2014). It can be denoted as

$$C_{\mathrm{R}}(\boldsymbol{x},\ m)=\frac{\sigma_{\hat{G}_m}(\boldsymbol{x})}{\left|\hat{G}_H(\boldsymbol{x})-\hat{G}_m(\boldsymbol{x})\right|+\sigma_{\hat{G}_H}(\boldsymbol{x})},\quad (14)$$

where $\sigma_{\hat{G}_H}(\boldsymbol{x})$ is larger than $\sigma_{\hat{G}_m}(\boldsymbol{x})$ because the uncertainty is transmitted along each recursive step. When $m\geqslant 2$, the predicted variance of $\sigma_{\hat{G}_m}(\boldsymbol{x})$ can be obtained through

$$p\left(\hat{G}_m(\boldsymbol{x})\right)=\int p\left(\boldsymbol{x},\ \hat{G}_{m-1}(\boldsymbol{x})\right)p\left(\hat{G}_{m-1}(\boldsymbol{x})\right)\mathrm{d}\boldsymbol{x},\quad (15)$$

where $p\left(\hat{G}_{m-1}(\boldsymbol{x})\right)$ is the posterior distribution of the previous fidelity level and $\sigma_{\hat{G}_m}(\boldsymbol{x})$ is obtained by calculating its confidence interval. To alleviate the computational burden associated with computing Monte Carlo integrals for all candidate samples, $\sigma_{\hat{G}_m}(\boldsymbol{x})$ is estimated as

$$\sigma_{\hat{G}_m}(\boldsymbol{x})=\sum_{q=1}^{m}\sigma_{\hat{G}}^{(q)}(\boldsymbol{x}),\quad (16)$$

where $\sigma_{\hat{G}}^{(q)}(\cdot)$ is the standard deviation of the Kriging model when the fidelity level is equal to q. $C_{\mathrm{R}}(\boldsymbol{x},\ m)$ is applied to characterize the acceptance of low-fidelity samples. When $m=H$, $C_{\mathrm{R}}(\boldsymbol{x},\ m)$ is equal to 1.

3.4.2 Stopping criterion

A conservative stopping criterion can result in unnecessary evaluations of the expensive limit state function, whereas premature termination of the sampling process may lead to incorrect estimation of the failure probability. To achieve fast convergence, the efficient error-based stopping criterion (ESC) (Wang and Shafieezadeh, 2019a) was extended for use in multi-source information scenarios. Based on the upper limit of the relative error, the ESC is defined as

$$\varepsilon=\left|\frac{\hat{N}_{\mathrm{f}}}{N_{\mathrm{f}}}-1\right|\leqslant \max\left(\left|\frac{\hat{N}_{\mathrm{f}}}{\hat{N}_{\mathrm{f}}-\hat{S}_{\mathrm{f}}^{\mathrm{u}}}-1\right|,\left|\frac{\hat{N}_{\mathrm{f}}}{\hat{N}_{\mathrm{f}}+\hat{S}_{\mathrm{s}}^{\mathrm{u}}}-1\right|\right)=\hat{\varepsilon}_{\max}, \tag{17}$$

where N_{f} and $\hat{N}_{\mathrm{f}}$ denote the numbers of real and estimated failure samples, respectively; $\hat{S}_{\mathrm{f}}$ is the estimated number of samples that are actually failed among all samples that are judged to be safe; $\hat{S}_{\mathrm{s}}$ is the estimated number of samples that are actually safe among all samples that are judged to be failed; $\hat{S}_{\mathrm{f}}^{\mathrm{u}}$ and $\hat{S}_{\mathrm{s}}^{\mathrm{u}}$ are the upper bounds of the confidence intervals of $\hat{S}_{\mathrm{f}}$ and $\hat{S}_{\mathrm{s}}$, respectively; $\hat{\varepsilon}_{\max}$ is the specified threshold, whose detailed calculation process can be found in Section S2 of the ESM.

3.5 Steps of the proposed method

The details of the application steps are as follows:

Step 1: Generate initial samples $\{\boldsymbol{X}_m\}_{m=1}$ by EVOP-LHS, and select samples $\{\boldsymbol{X}_m\}_{m=2,3,\cdots,H}$ by the exchange algorithm (Forrester et al., 2007).

Step 2: Generate the Monte Carlo population $\boldsymbol{S}$ according to the statistical characteristics of the design variables.

Step 3: Construct (update) the residual model $F_{\mathrm{Re}}(\cdot)$ according to current samples with different fidelities and their response values.

Step 4: Calculate response values of nested samples based on $F_{\mathrm{Re}}(\cdot)$.

Step 5: Construct (update) the NAMK model using current samples with different fidelities and their response values.

Step 6: Calculate the predicted values using the constructed NAMK model, and estimate the failure probability by $\hat{p}_{\mathrm{f}}=\frac{1}{N_{\mathrm{MCS}}}\sum_{i=1}^{N_{\mathrm{MCS}}}I\left(\hat{G}_H(\boldsymbol{x}_i)\right)$, where $I\left(\hat{G}_H(\boldsymbol{x}_i)\right)=0$ when $\hat{G}_H(\boldsymbol{x}_i)>0$, and $I\left(\hat{G}_H(\boldsymbol{x}_i)\right)=1$ when $\hat{G}_H(\boldsymbol{x}_i)\leqslant 0$.

Step 7: Estimate the maximum error according to $\boldsymbol{S}$.

Step 8: Check the stopping criterion. If the stopping condition is met, turn to Step 10; otherwise, turn to Step 9.

Step 9: Determine the location and fidelity of the new sample by $\{\boldsymbol{x}^{\mathrm{new}}, m^{\mathrm{new}}\}=\arg\max_{\boldsymbol{x},\, m}\left(F_{\mathrm{MF}}(\boldsymbol{x}, m)\right)$, and update the training sample set.

Step 10: Check the coefficient of variation by $\mathrm{COV}=\sqrt{\frac{1-\hat{p}_{\mathrm{f}}}{N_{\mathrm{MCS}}\hat{p}_{\mathrm{f}}}}$. If $\mathrm{COV}\leqslant 0.05$, turn to Step 12; otherwise, turn to Step 11.

Step 11: Update $\boldsymbol{S}$ by adding extra candidate samples, and turn to Step 2.

Step 12: Report $\hat{p}_{\mathrm{f}}$.

4 Case studies

To assess the accuracy and efficiency of the proposed approach, we investigated three numerical cases of variable complexity, as well as an engineering case. The code was implemented in MATLAB, and the Kriging model was constructed using the DACE toolbox (Lophaven et al., 2002). Several state-of-the-art methods for reliability analysis methods based on surrogate modeling were adopted for comparison: (1) EGRA (Bichon et al., 2008), (2) AK-MCS+U (Echard et al., 2013), (3) REAK (Wang and Shafieezadeh, 2019b), (4) AKOIS (Zhang et al., 2020), (5) mfEGRA (Chaudhuri et al., 2021), and (6) AMK-MCS+AEFF (Liu et al., 2022). Among these methods, AK-MCS+U is the AK-MCS method using the U learning function, and AMK-MCS+AEFF is the multi-fidelity AK-MCS method using a learning function called AEFF. The efficiency of these methods was compared in terms of the average cost considering all fidelity samples, and their accuracy was quantified using the average relative error of failure probability, which can be characterized as

$$\eta=\frac{1}{n_{\mathrm{r}}}\sum_{i=1}^{n_{\mathrm{r}}}\left|\,p_{\mathrm{f}}^{\mathrm{MCS}}-\hat{p}_{\mathrm{f}}^{(i)}\,\right|, \tag{18}$$

where n_{r} is the number of repeated calculations, $p_{\mathrm{f}}^{\mathrm{MCS}}$ is the failure probability obtained by MCS method, and $\hat{p}_{\mathrm{f}}^{(i)}$ represents the ith estimated failure probability. To achieve a robust result, all methods were performed 10 times for each case.

4.1 Example 1: multimodal function

In this example, the multimodal function (Bichon et al., 2008), a classical test function in the field of reliability, was used to demonstrate the active learning process in detail and assess the effectiveness of the proposed method. The high-fidelity model of the limit state function is defined by

$$f_3(\boldsymbol{x}) = 2 - \frac{(x_1^2+4)(x_2-1)}{20} - \sin\left(\frac{5x_1}{2}\right), \quad (19)$$

where x_1 is normally distributed with a mean value of 1.5 and a variance of 1, and x_2 is normally distributed with a mean value of 2.5 and a variance of 1. The two low-fidelity models (Chaudhuri et al., 2021) were represented as

$$f_2(\boldsymbol{x}) = f_3(\boldsymbol{x}) + \sin\left(\frac{5x_1}{22} + \frac{5x_2}{44} + \frac{5}{4}\right), \quad (20)$$

$$f_1(\boldsymbol{x}) = f_3(\boldsymbol{x}) + 3\sin\left(\frac{5x_1}{11} + \frac{5x_2}{11} + \frac{35}{11}\right). \quad (21)$$

Assume that the cost of each fidelity model remains the same throughout the domain. The costs are $c(3)$=1, $c(2)$=0.1, and $c(1)$=0.01 (Marques et al., 2018). The contour plots of three fidelity models in the demonstration case and the limit state function of each model are shown in Fig. 3.

Fig. 4 shows several iterations of the random running sequential process of the proposed scheme. Fig. 4a depicts the position of the initial samples with variable fidelity. The proposed method first generates 24 samples with fidelity level m=1 from the design space $[\mu-5\sigma, \mu+5\sigma]$ by EVOP-LHS and then selects

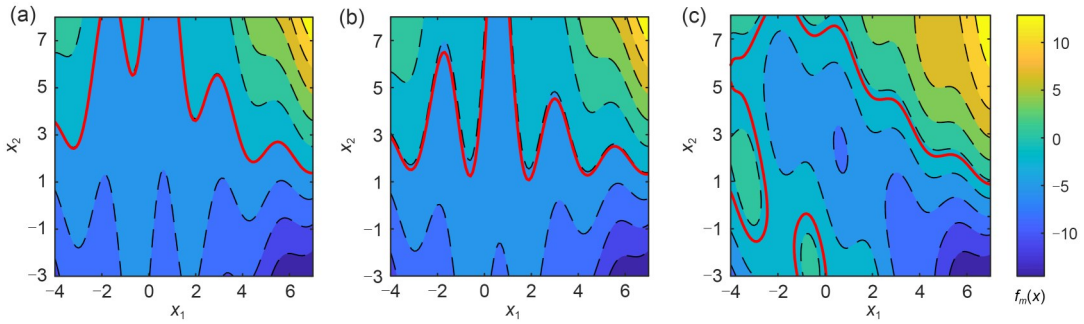

Fig. 3 Contours of $f_m(x)$ using the three fidelity models for the multimodal function (solid line represents the limit state plane): (a) fidelity level m=3; (b) fidelity level m=2; (c) fidelity level m=1

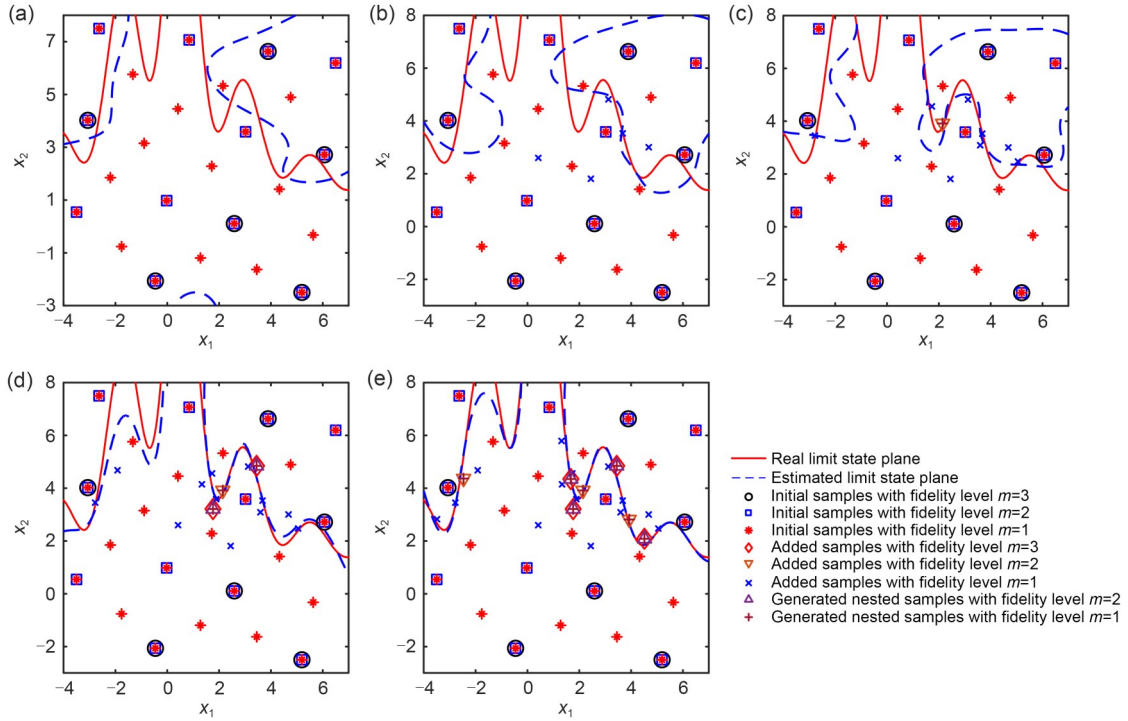

Fig. 4 Iteration process of the proposed method on the multimodal function: (a) iteration 0; (b) iteration 5; (c) iteration 10; (d) iteration 15; (e) the last iteration (iteration 21)

12 samples with fidelity level m=2 and six samples with fidelity level m=3 by the exchange algorithm, where μ and σ are the mean and standard deviation of random variables, respectively. Figs. 4b–4e show the process of selecting new samples, generating nested samples and the iterative process of the contour. As illustrated in Figs. 4b and 4c, the proposed method tends to prioritize the selection of low-fidelity samples in the initial iterations due to the limited knowledge of the limit state. This cautious approach allows for a broader exploration of the design space and facilitates the acquisition of crucial information about the system's behavior. However, as understanding of the limit state deepens, the method gradually shifts towards selecting high-fidelity samples in the later iterations, as observed in Figs. 4d and 4e. This adaptive sampling strategy allows the method to focus on areas of higher uncertainty and refine the surrogate model for more accurate predictions. In addition, because of the $U_{\mathrm{MF}}(\boldsymbol{x})$, the points explored in the active learning process are concentrated mainly near the limit state, which is conducive to a more accurate evaluation of the failure probability. Consequently, the limit state plane evaluated by the NAMK model accurately tracks the actual failure boundary (Fig. 4e). The performance of the proposed approach was compared with MCS, EGRA, AK-MCS+U, REAK, AKOIS, mfEGRA, and AMK-MCS+AEFF. The results of these comparisons are summarized in Table 1.

As listed in Table 1, the cost of the proposed method was 12.90, which was the lowest among all methods. The relative error of the proposed method was merely 0.97%, outperforming AKOIS, mfEGRA, and AMK-MCS+AEFF in accuracy. Notably, while AK-MCS+U achieved high accuracy, its computational cost of 39.2 was 3.04 times higher than that of our method. Compared to single-fidelity active learning methods such as EGRA and REAK, our method significantly reduced the cost while maintaining similar accuracy levels. To further prove the robustness of the proposed method, Fig. 5 shows boxplots of all the listed methods in terms of total cost and relative error. Our proposed method showed good stability in both efficiency and accuracy due to the use of the ESC.

4.2 Example 2: 4D PARK function

For the second example, we used the 4D PARK function (Cutajar et al., 2019) to validate the effectiveness of the proposed method in highly nonlinear problems. The 4D PARK function can be expressed as

$$f_2(\boldsymbol{x}) = \frac{x_1}{2}\left[\sqrt{(x_2+x_3^2)\frac{x_4}{x_1^2}+1}-1\right]+ (x_1+3x_4)\exp[\sin(x_3)+1]-2, \tag{22}$$

$$f_1(\boldsymbol{x}) = \left[\frac{\sin(x_1)}{10}+1\right]f_2(\boldsymbol{x})+x_2^2+x_3^2-2x_1+0.5, \tag{23}$$

where $f_2(\boldsymbol{x})$ is the high-fidelity model, and $f_1(\boldsymbol{x})$ is the low-fidelity model. All inputs obey the uniform distribution of $[0, 1]$, and the costs are set to $c(2)$=1 and $c(1)$=0.1. The running results of the different methods applied to this example are shown in Table 2.

Table 2 shows that our proposed method effectively leverages multi-fidelity samples to establish a precise mapping between low-fidelity and high-fidelity samples, thereby significantly reducing computational overhead and delivering accurate failure probability estimates. In terms of efficiency, our method surpassed all others, incurring a calculation cost of only 28.70. Regarding accuracy, while the calculation error of our method was marginally higher than those of AK-MCS+U, REAK, and AKOIS, its computational cost was 48.0%, 67.1%, and 60.7% lower, respectively. Furthermore, due to the pronounced nonlinear relationship

Table 1 Results of different methods for the multimodal function

Method	Cost	$\hat{p}_{\mathrm{f}}$ ($\times10^{-2}$)	COV (%)	Error (%)
MCS	10^6	3.13	0.56	–
EGRA	49.3	3.14	3.93	0.24
AK-MCS+U	39.2	3.13	3.93	2.84×10^{-2}
REAK	28.6	3.14	3.92	0.74
AKOIS	30.8	3.16	3.90	1.13
mfEGRA	15.24 (12.1+26.6×0.1+47.9×0.01)	3.09	3.96	1.45
AMK-MCS+AEFF	14.9 (10.3+46×0.1)	3.12	3.93	1.15
Proposed method	12.90 (10.9+16.1×0.1+39.2×0.01)	3.12	3.89	0.97

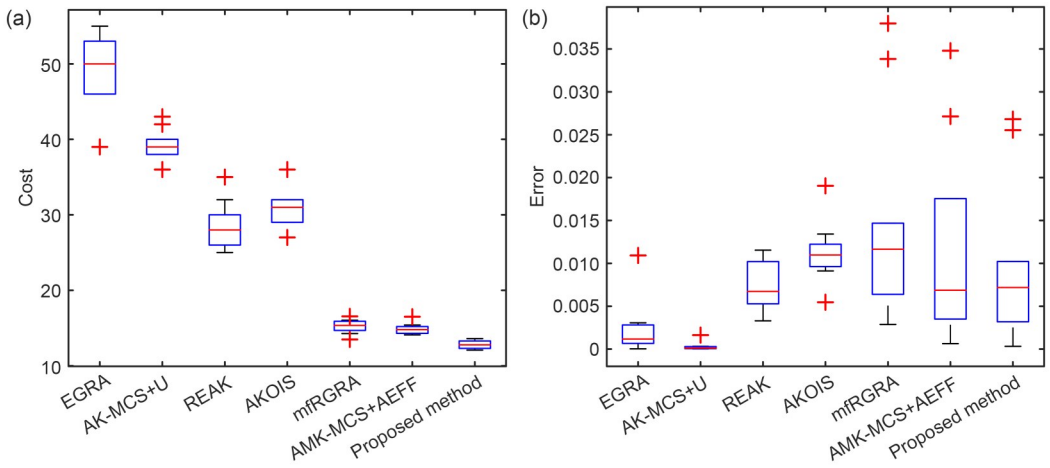

Fig. 5 Boxplots of cost (a) and relative error (b) of different methods

Table 2 Results of different methods for the 4D PARK function

Method	Cost	$\hat{p}_f$ ($\times10^{-2}$)	COV (%)	Error (%)
MCS	1×10^6	3.86	0.50	–
EGRA	72.2	3.92	3.50	2.01
AK-MCS+U	59.8	3.86	3.52	0.13
REAK	42.8	3.87	3.52	0.36
AKOIS	47.3	3.84	3.54	0.48
mfEGRA	40.15 (30.6+95.5×0.1)	3.73	3.60	5.80
AMK-MCS+AEFF	38.71 (29.8+89.1×0.1)	3.81	3.55	2.13
Proposed method	28.70 (22.5+62.0×0.1)	3.85	3.54	0.51

between the high-fidelity and low-fidelity models, mfRGRA and AK-MCS+U failed to achieve satisfactory accuracy, highlighting the importance of accurately capturing the nonlinear relationship in multi-fidelity modeling.

4.3 Example 3: vehicle side impact problem

In this section, we assess the accuracy and efficiency of the proposed scheme in tackling complex problems by using the vehicle side impact problem (Youn et al., 2004; Yi et al., 2021) as a case study. This problem is characterized by a seven-dimensional limit state function, which can be represented as

$$f_2(\boldsymbol{x}) = 0.489x_1x_4 + 0.843x_2x_3 - 0.0432x_5x_6 + 0.0556x_5x_7 + 0.00078x_7^2 - 0.75, \tag{24}$$

$$\begin{aligned} f_1(\boldsymbol{x}) = f_2(\boldsymbol{x}) - \frac{1}{10}(&0.489(x_1-0.1)(x_4-0.1) + \\ &0.843(x_2-0.1)(x_3-0.1) + \\ &0.0432(x_2-0.1)(x_3-0.1) + \\ &0.0556(x_5-0.1)(x_7-0.1) + \\ &0.00078(x_7-1)), \end{aligned} \tag{25}$$

where $f_2(\boldsymbol{x})$ is the high-fidelity model, and $f_1(\boldsymbol{x})$ is the low-fidelity model. The statistical characteristics of $\boldsymbol{x}$ are shown in Table 3, and the costs were set to $c(2)$=1 and $c(1)$=0.05 (Yi et al., 2021). Table 4 summarizes the running results of different methods applied to this problem.

Table 3 Distributions and parameters of x of the vehicle side impact problem

Variable	Mean	Standard deviation	Distribution	Description
x_1	1.38	0.30	Normal	Floor side inner
x_2	1.38	0.30	Normal	Door beam
x_3	1.38	0.30	Normal	Door beltline
x_4	1.38	0.30	Normal	Roof rail
x_5	0.30	0.06	Normal	Floor side inner
x_6	0	10	Normal	Barrier height
x_7	0	10	Normal	Barrier hitting

Table 4 shows that, compared to other single-fidelity active learning methods, the calculation error of our proposed method was 1.19%, slightly exceeding that of AK-MCS+U, REAK, and AKOIS, but its

cost was obviously reduced. Furthermore, owing to the NAMK model's efficient capture of the nonlinear relationship between multi-fidelity samples, our method outperformed other multi-fidelity modeling methods, including mfEGRA and AMK-MCS+AEFF, in both computational cost and efficiency. Fig. 6 provides a comparison of the convergence of the relative error of failure probability for the different methods. Our proposed method achieved a lower relative error level with a relatively small number of calculations, indicating its superior convergence performance in this case.

4.4 Engineering application: aircraft tubing

Tubing assembly is widely used in aircraft subsystems (e.g., hydraulic systems, fuel systems, and environmental control systems) and significantly influences aircraft reliability and safety. In this case, we investigated the reliability analysis of the overall stability of aircraft tubing (Li and Wang, 2019) to demonstrate the practicality of the proposed method in engineering problems. The structural profile of the tubing is visually depicted in Fig. 7, illustrating its geometric configuration and layout. Additionally, Table 5 provides an overview of the statistical characteristics associated with the structural parameters relevant to the tubing. The tubing is constructed from steel material with a Poisson's ratio of 0.27 and Young's modulus of 200 GPa, and a pressure of P=33 MPa was applied to the inner surface. The critical threshold of failure was defined as a maximum total deformation of tubing greater than 0.01 mm.

In this work, the finite element method (FEM) was used to obtain the maximum deformation of the tubing. In the analysis of the tubing assembly, two different mesh configurations were used: a fine mesh and a coarse mesh. The solution obtained from the fine mesh was considered the high-fidelity model, which provided more accurate and detailed results. The solution obtained from the coarse mesh was regarded as the

Table 4 Results of different methods for the vehicle side impact problem

Method	Cost	$\hat{p}_f$ ($\times10^{-4}$)	COV (%)	Error (%)
MCS	5×10^6	1.64	3.49	–
EGRA	79.9	1.74	3.39	6.86
AK-MCS+U	91.8	1.65	3.49	0.55
REAK	65.2	1.62	3.51	1.09
AKOIS	58.0	1.65	3.48	0.82
mfEGRA	53.9 (48.4+109.3×0.05)	1.60	3.54	2.41
AMK-MCS+AEFF	49.5 (42.6+137.2×0.05)	1.61	3.52	1.28
Proposed method	37.6 (33.6+80.4×0.05)	1.67	3.48	1.19

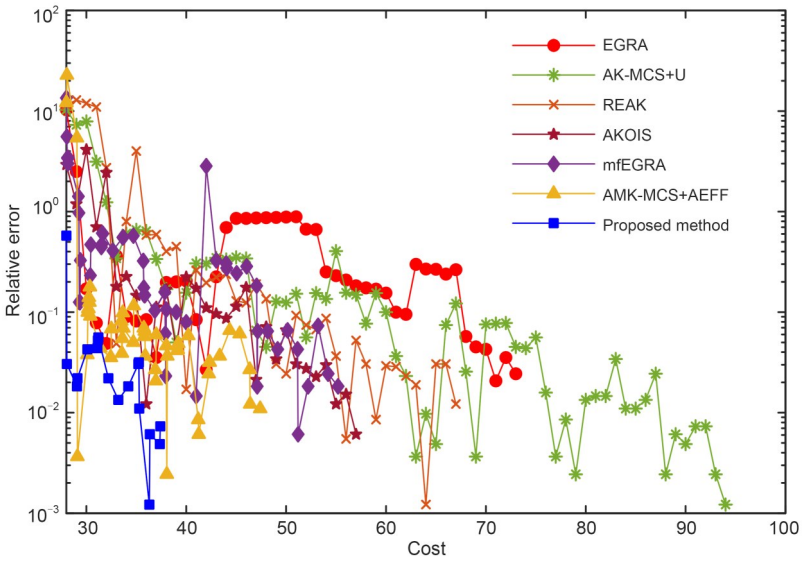

Fig. 6 Relative errors of failure probability of different methods (shown in log-scale)

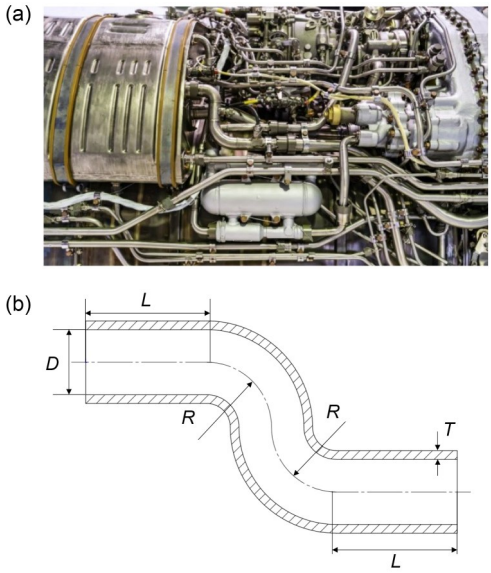

Fig. 7 Aircraft tubing: (a) aircraft fuel system; (b) geometry of the aircraft tubing

low-fidelity model, which provided approximate results with reduced computational cost. The commercial software ABAQUS was used to carry out the finite element analysis. For the high-fidelity model, a mesh consisting of 18432 elements was used to ensure accurate results. Conversely, a mesh model with only 880 elements was used as the low-fidelity model to facilitate faster computations. The mesh of the high-fidelity model is depicted in Fig. 8a, while that of the low-fidelity model is shown in Fig. 8b.

Table 5 Statistical characteristics of variables of the aircraft tubing

Variable	Meaning	Mean (mm)	Standard deviation (mm)	Distribution
D	Inner diameter	17.0	0.2	Normal
T	Thickness	2.98	0.05	Normal
R	Radius of bending	2.93	0.11	Lognormal
L	Length	3.56	0.02	Lognormal

Fig. 9 illustrates the deformation simulation results obtained from the different fidelity models. Similar displacement distributions in Figs. 9a and 9b indicate

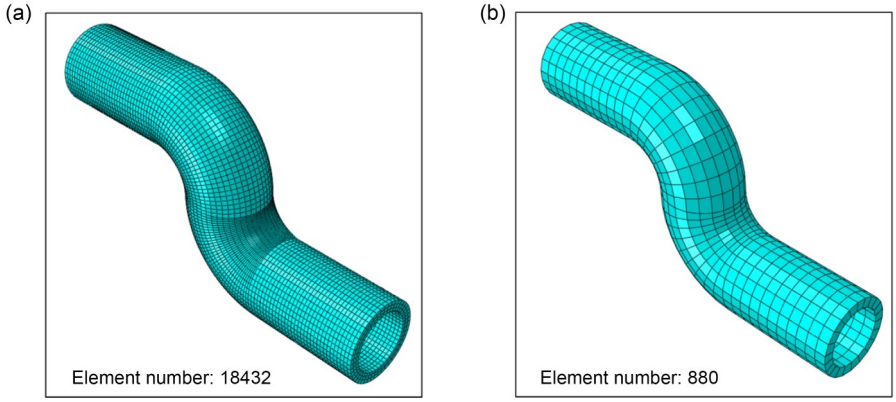

Fig. 8 Mesh grids of the high-fidelity finite element model (a) and low-fidelity finite element model (b)

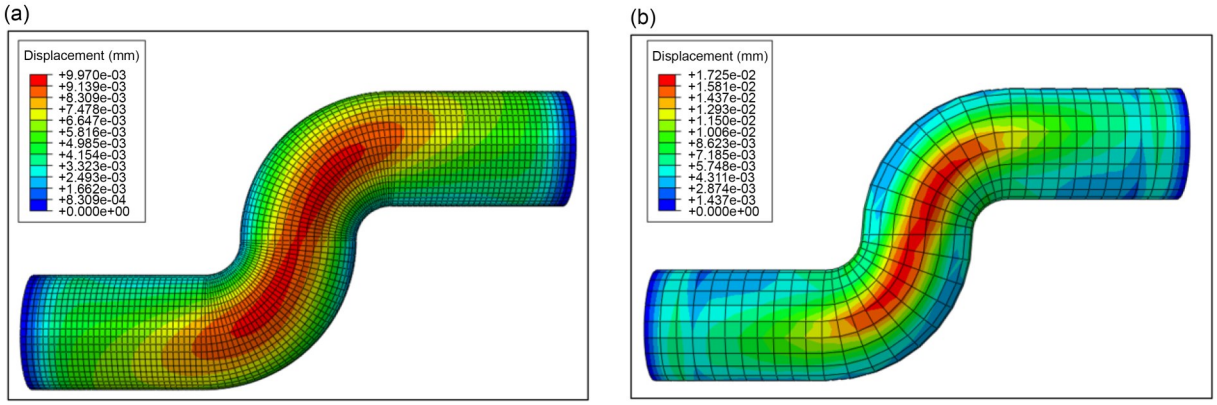

Fig. 9 Simulation results of the high-fidelity model (a) and low-fidelity model (b)

that using the low-fidelity model was a reasonable simplification method. Moreover, the high-fidelity and low-fidelity model simulation times were 17.2 s and 2.1 s, respectively. Therefore, the costs were set to $c(2)=1$ and $c(1)=1/8$. Table 6 presents the results of the different methods for reliability analysis of aircraft tubing.

Table 6 Results of different methods for the aircraft tubing problem

Method	Cost	$\hat{p}_f$ ($\times10^{-2}$)	COV (%)	Error (%)
MCS	1×10^4	4.92	4.41	–
EGRA	43.9	4.72	4.51	5.09
AK-MCS+U	38.5	4.93	4.39	0.66
REAK	34.1	4.95	4.36	0.80
AKOIS	37.9	4.96	4.35	1.12
mfEGRA	26.2 (20.6+44.8×1/8)	4.87	4.64	2.10
AMK-MCS+AEFF	23.6 (17.6+48.2×1/8)	4.96	4.36	1.41
Proposed method	18.8 (14.7+32.6×1/8)	4.90	4.43	1.07

From the results provided in Table 6, we conclude that our proposed method had the best efficiency among all the methods. In terms of the calculation error, the relative error of our proposed method was 1.07%, which was only slightly larger than those of AK-MCS+U and REAK, and their calculation costs were several times that of our proposed method. In summary, our proposed method showed excellent performance in this engineering application.

5 Conclusions

In this paper, we propose a novel NAMK-based method with active learning for efficient and accurate reliability analysis. This method leverages NAMK modeling to accurately capture nonlinear relationships between multi-fidelity samples. This can improve the generalization performance of a surrogate model. A multi-fidelity learning function considering the correlation and sampling cost of various fidelity samples can adaptively determine the position and fidelity of the new sample. When a high-fidelity sample is selected by the learning function, the constructed residual model used to generate a nested low-fidelity sample reduces the calls of the low-fidelity model.

The performance of the proposed method was verified using three benchmark numerical examples of variable complexity, as well as an engineering example. Compared to EGRA, AK-MCS+U, REAK, and AKOIS, the proposed method showed effective use of multi-source information, resulting in a significant reduction in the number of high-fidelity samples while maintaining calculation accuracy. Additionally, the proposed method exhibited improved accuracy in capturing the nonlinear relationship between samples of different fidelities compared to mfEGRA and AMK-MCS+AEFF. Moreover, during the model updating process, the proposed method required fewer low-fidelity samples compared to mfEGRA and AMK-MCS+AEFF. These advantages make the proposed method a promising approach for handling reliability analysis problems.

Although the proposed method has proven effective for general reliability analysis problems, its use could be further extended to address hybrid reliability analysis problems that involve both random and interval variables. Moreover, the basic framework of the proposed method could be enhanced by incorporating dimension reduction methods (Zhou and Peng, 2020a; Ji et al., 2022) to address high-dimensional reliability analysis problems.

Acknowledgments

This work is supported by the Major Projects of Zhejiang Provincial Natural Science Foundation of China (No. LD22E050009), the National Natural Science Foundation of China (No. 51475425), and the College Student's Science and Technology Innovation Project of Zhejiang Province (No. 2022R403B060), China.

Author contributions

Yifan LI devised the methodology, developed the software, validated the results, and wrote the initial draft. Yongyong XIANG optimized the methodology and revised the manuscript. Luojie SHI optimized the software and revised the manuscript. Baisong PAN conceived the methodology and edited the final version.

Conflict of interest

Yifan LI, Yongyong XIANG, Luojie SHI, and Baisong PAN declare that they have no conflict of interest.

References

Aldosary M, Wang JS, Li CF, 2018. Structural reliability and stochastic finite element methods: state-of-the-art review

and evidence-based comparison. *Engineering Computations*, 35(6):2165-2214. https://doi.org/10.1108/EC-04-2018-0157

Bichon BJ, Eldred MS, Swiler LP, et al., 2008. Efficient global reliability analysis for nonlinear implicit performance functions. *AIAA Journal*, 46(10):2459-2468. https://doi.org/10.2514/1.34321

Chaudhuri A, Marques AN, Willcox K, 2021. mfEGRA: multifidelity efficient global reliability analysis through active learning for failure boundary location. *Structural and Multidisciplinary Optimization*, 64(2):797-811. https://doi.org/10.1007/s00158-021-02892-5

Chen J, Gao Y, Liu YM, 2022. Multi-fidelity data aggregation using convolutional neural networks. *Computer Methods in Applied Mechanics and Engineering*, 391:114490. https://doi.org/10.1016/j.cma.2021.114490

Cheng J, Li QS, 2008. Reliability analysis of structures using artificial neural network based genetic algorithms. *Computer Methods in Applied Mechanics and Engineering*, 197(45-48):3742-3750. https://doi.org/10.1016/j.cma.2008.02.026

Cutajar K, Pullin M, Damianou A, et al., 2019. Deep Gaussian processes for multi-fidelity modeling. arXiv:1903.07320. https://doi.org/10.48550/arXiv.1903.07320

Echard B, Gayton N, Lemaire M, 2011. AK-MCS: an active learning reliability method combining Kriging and Monte Carlo simulation. *Structural Safety*, 33(2):145-154. https://doi.org/10.1016/j.strusafe.2011.01.002

Echard B, Gayton N, Lemaire M, et al., 2013. A combined importance sampling and Kriging reliability method for small failure probabilities with time-demanding numerical models. *Reliability Engineering & System Safety*, 111:232-240. https://doi.org/10.1016/j.ress.2012.10.008

Feng JW, Liu L, Wu D, et al., 2019. Dynamic reliability analysis using the extended support vector regression (X-SVR). *Mechanical Systems and Signal Processing*, 126:368-391. https://doi.org/10.1016/j.ymssp.2019.02.027

Forrester AIJ, Sóbester A, Keane AJ, 2007. Multi-fidelity optimization via surrogate modelling. *Proceedings of the Royal Society A: Mathematical, Physical and Engineering Sciences*, 463(2088):3251-3269. https://doi.org/10.1098/rspa.2007.1900

Forrester AIJ, Sóbester A, Keane AJ, 2008. Engineering Design via Surrogate Modelling: a Practical Guide. John Wiley & Sons, Hoboken, USA. https://doi.org/10.1002/9780470770801

Gavin HP, Yau SC, 2008. High-order limit state functions in the response surface method for structural reliability analysis. *Structural Safety*, 30(2):162-179. https://doi.org/10.1016/j.strusafe.2006.10.003

Goswami S, Ghosh S, Chakraborty S, 2016. Reliability analysis of structures by iterative improved response surface method. *Structural Safety*, 60:56-66. https://doi.org/10.1016/j.strusafe.2016.02.002

Guo MW, Manzoni A, Amendt M, et al., 2022. Multi-fidelity regression using artificial neural networks: efficient approximation of parameter-dependent output quantities. *Computer Methods in Applied Mechanics and Engineering*, 389:114378. https://doi.org/10.1016/j.cma.2021.114378

He WX, Zeng Y, Li G, 2020. An adaptive polynomial chaos expansion for high-dimensional reliability analysis. *Structural and Multidisciplinary Optimization*, 62(4):2051-2067. https://doi.org/10.1007/s00158-020-02594-4

Hohenbichler M, Rackwitz R, 1982. First-order concepts in system reliability. *Structural Safety*, 1(3):177-188. https://doi.org/10.1016/0167-4730(82)90024-8

Hong HP, 1996. Point-estimate moment-based reliability analysis. *Civil Engineering Systems*, 13(4):281-294. https://doi.org/10.1080/02630259608970204

Hong LX, Li HC, Fu JF, 2022. A novel surrogate-model based active learning method for structural reliability analysis. *Computer Methods in Applied Mechanics and Engineering*, 394:114835. https://doi.org/10.1016/j.cma.2022.114835

Hu C, Youn BD, 2011. Adaptive-sparse polynomial chaos expansion for reliability analysis and design of complex engineering systems. *Structural and Multidisciplinary Optimization*, 43(3):419-442. https://doi.org/10.1007/s00158-010-0568-9

Ji YX, Xiao NC, Zhan HY, 2022. High dimensional reliability analysis based on combinations of adaptive Kriging and dimension reduction technique. *Quality and Reliability Engineering International*, 38(5):2566-2585. https://doi.org/10.1002/qre.3091

Jones DR, Schonlau M, Welch WJ, 1998. Efficient global optimization of expensive black-box functions. *Journal of Global optimization*, 13(4):455-492. https://doi.org/10.1023/A:1008306431147

Kaymaz I, 2005. Application of Kriging method to structural reliability problems. *Structural Safety*, 27(2):133-151. https://doi.org/10.1016/j.strusafe.2004.09.001

Kennedy MC, O'Hagan A, 2000. Predicting the output from a complex computer code when fast approximations are available. *Biometrika*, 87(1):1-13. https://doi.org/10.1093/biomet/87.1.1

Kiureghian AD, Stefano MD, 1991. Efficient algorithm for second-order reliability analysis. *Journal of Engineering Mechanics*, 117(12):2904-2923. https://doi.org/10.1061/(ASCE)0733-9399(1991)117:12(2904)

Krige DG, 1951. A statistical approach to some basic mine valuation problems on the Witwatersrand. *Journal of the Southern African Institute of Mining and Metallurgy*, 52(6):119-139.

Le Gratiet L, Garnier J, 2014. Recursive co-Kriging model for design of computer experiments with multiple levels of fidelity. *International Journal for Uncertainty Quantification*, 4(5):365-386. https://doi.org/10.1615/Int.J.UncertaintyQuantification.

2014006914

Lelièvre N, Beaurepaire P, Mattrand C, et al., 2018. AK-MCSi: a Kriging-based method to deal with small failure probabilities and time-consuming models. *Structural Safety*, 73:1-11. https://doi.org/10.1016/j.strusafe.2018.01.002

Li HS, Cao ZJ, 2016. Matlab codes of subset simulation for reliability analysis and structural optimization. *Structural and Multidisciplinary Optimization*, 54(2):391-410. https://doi.org/10.1007/s00158-016-1414-5

Li MY, Wang ZQ, 2019. Surrogate model uncertainty quantification for reliability-based design optimization. *Reliability Engineering & System Safety*, 192:106432. https://doi.org/10.1016/j.ress.2019.03.039

Li X, Gong CL, Gu LX, et al., 2018. A sequential surrogate method for reliability analysis based on radial basis function. *Structural Safety*, 73:42-53. https://doi.org/10.1016/j.strusafe.2018.02.005

Liu J, Yi JX, Zhou Q, et al., 2022. A sequential multi-fidelity surrogate model-assisted contour prediction method for engineering problems with expensive simulations. *Engineering with Computers*, 38(1):31-49. https://doi.org/10.1007/s00366-020-01043-6

Lophaven SN, Nielsen HB, Søndergaard J, 2002. DACE– a Matlab Kriging Toolbox, Version 2.0. Technical Report No. IMM-TR-2002-12, Technical University of Denmark, Kongens Lyngby, Denmark.

Marques AN, Lam RR, Willcox KE, 2018. Contour location via entropy reduction leveraging multiple information sources. Proceedings of the 32nd International Conference on Neural Information Processing Systems, p.5223-5233.

Melchers RE, 1990. Radial importance sampling for structural reliability. *Journal of Engineering Mechanics*, 116(1): 189-203. https://doi.org/10.1061/(ASCE)0733-9399(1990)116:1(189)

Meng XH, Karniadakis GE, 2020. A composite neural network that learns from multi-fidelity data: application to function approximation and inverse PDE problems. *Journal of Computational Physics*, 401:109020. https://doi.org/10.1016/j.jcp.2019.109020

Papaioannou I, Papadimitriou C, Straub D, 2016. Sequential importance sampling for structural reliability analysis. *Structural Safety*, 62:66-75. https://doi.org/10.1016/j.strusafe.2016.06.002

Perdikaris P, Raissi M, Damianou A, et al., 2017. Nonlinear information fusion algorithms for data-efficient multi-fidelity modelling. *Proceedings of the Royal Society A: Mathematical, Physical and Engineering Sciences*, 473(2198): 20160751. https://doi.org/10.1098/rspa.2016.0751

Rajashekhar MR, Ellingwood BR, 1993. A new look at the response surface approach for reliability analysis. *Structural Safety*, 12(3):205-220. https://doi.org/10.1016/0167-4730(93)90003-J

Reisenthel PH, Allen TT, 2014. Application of multifidelity expected improvement algorithms to aeroelastic design optimization. The 10th AIAA Multidisciplinary Design Optimization Conference, article 1490. https://doi.org/10.2514/6.2014-1490

Ren C, Aoues Y, Lemosse D, et al., 2022. Ensemble of surrogates combining Kriging and artificial neural networks for reliability analysis with local goodness measurement. *Structural Safety*, 96:102186. https://doi.org/10.1016/j.strusafe.2022.102186

Roy A, Manna R, Chakraborty S, 2019. Support vector regression based metamodeling for structural reliability analysis. *Probabilistic Engineering Mechanics*, 55:78-89. https://doi.org/10.1016/j.probengmech.2018.11.001

Schuëller GI, Pradlwarter HJ, 2007. Benchmark study on reliability estimation in higher dimensions of structural systems–an overview. *Structural Safety*, 29(3):167-182. https://doi.org/10.1016/j.strusafe.2006.07.010

Song SF, Lu ZZ, Qiao HW, 2009. Subset simulation for structural reliability sensitivity analysis. *Reliability Engineering & System Safety*, 94(2):658-665. https://doi.org/10.1016/j.ress.2008.07.006

Su GS, Peng LF, Hu LH, 2017. A Gaussian process-based dynamic surrogate model for complex engineering structural reliability analysis. *Structural Safety*, 68:97-109. https://doi.org/10.1016/j.strusafe.2017.06.003

Wang JS, Li CF, Xu GJ, et al., 2021. Efficient structural reliability analysis based on adaptive Bayesian support vector regression. *Computer Methods in Applied Mechanics and Engineering*, 387:114172. https://doi.org/10.1016/j.cma.2021.114172

Wang ZY, Shafieezadeh A, 2019a. ESC: an efficient error-based stopping criterion for Kriging-based reliability analysis methods. *Structural and Multidisciplinary Optimization*, 59(5):1621-1637. https://doi.org/10.1007/s00158-018-2150-9

Wang ZY, Shafieezadeh A, 2019b. REAK: reliability analysis through error rate-based adaptive Kriging. *Reliability Engineering & System Safety*, 182:33-45. https://doi.org/10.1016/j.ress.2018.10.004

Wu HQ, Kuang SJ, Hou HB, 2019. Research on application of electric vehicle collision based on reliability optimization design method. *International Journal of Computational Methods*, 16(7):1950034. https://doi.org/10.1142/S0219876219500348

Yi JX, Wu FL, Zhou Q, et al., 2021. An active-learning method based on multi-fidelity Kriging model for structural reliability analysis. *Structural and Multidisciplinary Optimization*, 63(1):173-195. https://doi.org/10.1007/s00158-020-02678-1

Youn BD, Choi KK, Yang RJ, et al., 2004. Reliability-based design optimization for crashworthiness of vehicle side impact. *Structural and Multidisciplinary Optimization*, 26(3-4):272-283. https://doi.org/10.1007/s00158-003-0345-0

Zhang XF, Pandey MD, 2013. Structural reliability analysis based on the concepts of entropy, fractional moment and dimensional reduction method. *Structural Safety*, 43:28-40. https://doi.org/10.1016/j.strusafe.2013.03.001

Zhang XF, Wang L, Sørensen JD, 2020. AKOIS: an adaptive Kriging oriented importance sampling method for structural system reliability analysis. *Structural Safety*, 82: 101876. https://doi.org/10.1016/j.strusafe.2019.101876

Zhao H, Gao ZH, Xu F, et al., 2019. Review of robust aerodynamic design optimization for air vehicles. *Archives of Computational Methods in Engineering*, 26(3):685-732. https://doi.org/10.1007/s11831-018-9259-2

Zhou T, Peng YB, 2020a. Kernel principal component analysis-based Gaussian process regression modelling for high-dimensional reliability analysis. *Computers & Structures*, 241:106358. https://doi.org/10.1016/j.compstruc.2020.106358

Zhou T, Peng YB, 2020b. Structural reliability analysis via dimension reduction, adaptive sampling, and Monte Carlo simulation. *Structural and Multidisciplinary Optimization*, 62(5):2629-2651. https://doi.org/10.1007/s00158-020-02633-0

Electronic supplementary materials

Sections S1 and S2